Beating-Heart Robotic Surgery Using Bilateral Impedance Control: Theory and Experiments

Mojtaba Sharifi [1,2], Hassan Salarieh [1,*], Saeed Behzadipour [1], Mahdi Tavakoli [2]

[1] *Department of Mechanical Engineering, Sharif University of Technology, Tehran, Tehran, 11155-9567, Iran*

[2] *Department of Electrical and Computer Engineering, University of Alberta, Edmonton, Alberta, T6G 1H9 Canada*

** Corresponding author, Email: salarieh@sharif.edu, Phone: +98-21-66165538.*

Beating-Heart Robotic Surgery Using Bilateral Impedance Control: Theory and Experiments

Abstract

A bilateral impedance controller is presented to enable robot-assisted surgery of a beating heart. For this purpose, two desired impedance models are designed and realized for the master and slave robots interacting with the operator (surgeon) and the environment (heart tissue), respectively. The impedance models are designed such that (a) the slave robot complies with the oscillatory motion of the beating heart and (b) the surgeon perceives the non-oscillatory portion of the slave/heart contact force at the master robot implying arrested-heart surgery. These performance goals are achieved via appropriate adjustment of the impedance model parameters without any measurement or estimation of heart motion. Two nonlinear robust adaptive controllers are proposed for the master and slave robots to track their corresponding desired impedance responses in the Cartesian space. The stability, tracking convergence and the robustness against parametric and non-parametric modeling uncertainties are proven using the Lyapunov theorem and based on two types of adaptation laws. The stability of impedance models and nonlinear tele-operation system can enhance the patient's safety during the robotic surgery. Experimental results show that the proposed controller compensates for the beating motion and provides smooth force feedback to the surgeon.

Keywords: Beating-heart surgery, robotic surgery, bilateral impedance teleoperation control, nonlinear adaptive control.

1. Introduction

In recent years, teleoperation systems have been employed in biomedical applications such as minimally invasive robotic surgery [1], tele-rehabilitation [2-4] and tele-sonography [5, 6] systems. Teleoperation-based surgery of the heart as a moving organ is challenging due to its movement velocity and acceleration which are more than 210 mm/sec and 3800 mm/sec^2 at the mitral valve annulus, respectively [7].

Arresting the heart to perform the surgery has undesirable side effects such as increased stroke risk [8] and long-time cognitive decline [9]. If the heart is allowed to beat freely during the surgery, these side effects would be alleviated. Moreover, the normal beating motion of the heart during the surgery is helpful for physiologic *intraoperative* evaluation of reconstructive procedures on dynamic heart structures such as the mitral valve, which is not possible in the arrested-heart surgery. Beating-heart surgery can be facilitated via a master-slave teleoperation system in which the slave robot automatically complies with the heartbeat-induced motion of the heart while the surgeon operates through the master robot without needing to manually compensate for the heart's beating motion.

In the past decade, various control methods have been proposed for linear and nonlinear robotic teleoperation systems such as [10-14] for position and force tracking. However, they cannot be used in tele-surgery on a moving organ (e.g., the heart) which require a motion or force compensation strategy in addition to stable control laws.

Different strategies [15, 16] have been suggested for prediction and autonomous compensation of organ motion for robotic interactions using Model Predictive Control (MPC) methods and vision systems. Bachta et al. [17] have presented a piezo-actuated compliant mechanism for active stabilization of the beating heart using the MPC and H_∞ controllers. Bebek and Cavusoglu have measured the heart's position using sonomicrometry crystals [18] and a flexible whisker-like sensor [19] in order to not deal with ultrasound images, which involve acquisition and processing delays, for heart's position measurement. Ataollahi et al. [20] have also presented a new cardioscopic tool for optical imaging and tissue removal inside the beating-heart.

A Smith predictor [21] and Kalman filtering [22] were suggested recently to predict and compensate for the organ motion under delayed vision and ultrasound images, respectively. However, these visual based methods have some drawbacks such as a) requiring a vision and/or ultrasound imager to follow artificial or natural landmarks inside the heart tissue, b) during interactions with the surgical instrument, the heart's soft tissue deforms, which increases errors of the vision systems, and c) the processing of some vision data like the ultrasound images is time-consuming and generate considerable delays, which cause problems for the feedback control system.

Some other control strategies [1, 23-25] have been presented that do not have the above-mentioned drawbacks of visual-based position-control methods. The iterative learning control [26] and active observer (AOB) based force control [27] methods using Kalman Filter are used to compensate for the organ motion. The MPC method was also used as a linear predictive force controller [28] and its compensation performance was compared with the AOB approach in [29]. After that, a cascade force controller [30] was presented as a combination of the MPC and AOB approaches to compensate for physiological disturbances. Also, a force-based position tracking system [31, 32] was developed using a catheter robotic system and ultrasound observations of the previous motion cycles. Lastly, Hasanzadeh and Janabi-Sharifi [33] have employed a low-dimensional model for intracardiac catheters behavior in order to estimate the interaction force during heart surgeries. In the above force-based controllers, the convergence

and robustness of the observations/estimation algorithm together with the stability of employed controller were not proved analytically. Moreover, the rate of disturbance observation, estimation or prediction should be considerably faster than the heart rate in the above methods.

In this paper, a novel bilateral impedance control method is proposed for robotic surgery on the beating heart using the measured interaction forces and without any requirement for heart motion prediction, observation and/or learning. In this method, a virtual impedance model is defined and realized for the slave robot such that it can comply with the physiological force and/or disturbance of the beating heart while tracking the master robot's trajectory. Moreover, the surgeon can sense the non-oscillatory part of the slave/heart interaction force (such that the beating heart feels like a stationary heart) via implementing another impedance model for the master robot. Accordingly, the surgeon fatigue decreases and he/she does not need to manually compensate for the high-frequency oscillatory force and motion of the beating heart. For these purposes, the structure and parameters of the master and slave impedance models are designed such that they have desired responses with respect to the surgeon and heart forces.

The master and slave impedance models, that provide two relationships between the interaction forces and desired trajectories, are stable. These impedance models are realized for the multi-DOF master and slave robots with nonlinear dynamics using a bilateral adaptive controller. The stability of nonlinear tele-robotic system together with the proposed bilateral adaptive controller is proven via the Lyapunov method. Two kinds of adaptation laws are defined and employed in this controller to provide robustness against parametric and non-parametric modeling uncertainties of the system.

Accordingly, based on (a) the stability of impedance models, and (b) the Lyapunov-based stability proof for the proposed nonlinear robotic tele-surgery system, the patient safety can be enhanced during interaction with the slave robot using the presented impedance-based control strategy. Note that the communication delays are not considered in this work because the master/surgeon and slave/patient are close to each other in the most of real robot-assisted surgeries performed in medical clinics/hospitals. However, communication delays can be taken into account in future works for possible surgery operations on the remote patients.

2. Nonlinear Dynamics of a Master-Slave Robotic Surgery System

The nonlinear model of an *n*-DOF tele-robotic system (master and slave robots) with parametric (structured) and unstructured uncertainties is expressed in the joint space as (chapter 9 of [34]):

$$\mathbf{M}_{\mathbf{q},m}(\mathbf{q}_m)\ddot{\mathbf{q}}_m + \mathbf{C}_{\mathbf{q},m}(\mathbf{q}_m,\dot{\mathbf{q}}_m)\dot{\mathbf{q}}_m + \mathbf{G}_{\mathbf{q},m}(\mathbf{q}_m) + \mathbf{F}_{\mathbf{q},m}(\dot{\mathbf{q}}_m) = \boldsymbol{\tau}_m + \boldsymbol{\tau}_{sur} + \mathbf{d}_{\mathbf{q},m} \tag{1}$$

$$\mathbf{M}_{\mathbf{q},s}(\mathbf{q}_s)\ddot{\mathbf{q}}_s + \mathbf{C}_{\mathbf{q},s}(\mathbf{q}_s,\dot{\mathbf{q}}_s)\dot{\mathbf{q}}_s + \mathbf{G}_{\mathbf{q},s}(\mathbf{q}_s) + \mathbf{F}_{\mathbf{q},s}(\dot{\mathbf{q}}_s) = \boldsymbol{\tau}_s - \boldsymbol{\tau}_{env} + \mathbf{d}_{\mathbf{q},s} \tag{2}$$

where $\mathbf{q}_m$ and $\mathbf{q}_s \in \mathbb{R}^{n\times 1}$ are the joint positions, $\mathbf{M}_{\mathbf{q},m}(\mathbf{q}_m)$ and $\mathbf{M}_{\mathbf{q},s}(\mathbf{q}_s) \in \mathbb{R}^{n\times n}$ are the inertia/mass matrices, $\mathbf{C}_{\mathbf{q},m}(\mathbf{q}_m,\dot{\mathbf{q}}_m)$ and $\mathbf{C}_{\mathbf{q},s}(\mathbf{q}_s,\dot{\mathbf{q}}_s) \in \mathbb{R}^{n\times n}$ include the centrifugal and Coriolis terms, $\mathbf{G}_{\mathbf{q},m}(\mathbf{q}_m)$ and $\mathbf{G}_{\mathbf{q},s}(\mathbf{q}_s) \in \mathbb{R}^{n\times 1}$ are the gravity terms, $\mathbf{F}_{\mathbf{q},m}(\dot{\mathbf{q}}_m)$ and $\mathbf{F}_{\mathbf{q},s}(\dot{\mathbf{q}}_s) \in \mathbb{R}^{n\times 1}$ are the friction torques, and $\boldsymbol{\tau}_m$ and $\boldsymbol{\tau}_s \in \mathbb{R}^{n\times 1}$ are the control torques (originated from the actuators) of the master and the slave robots, respectively. Also, $\boldsymbol{\tau}_{sur} \in \mathbb{R}^{n\times 1}$ is the torque that the surgeon (human operator) applies to the master robot and $\boldsymbol{\tau}_{env} \in \mathbb{R}^{n\times 1}$ is the torque that the slave robot applies to the environment (heart tissue). The vectors of bounded unstructured modeling uncertainties and/or bounded exogenous disturbances of the system are also denoted by $\mathbf{d}_{\mathbf{q},m}$ and $\mathbf{d}_{\mathbf{q},s}$ for the master and slave robots, respectively. Then, the robots' end-effector equations of motion in the Cartesian space are represented as:

$$\mathbf{M}_{\mathbf{x},m}(\mathbf{q}_m)\ddot{\mathbf{x}}_m + \mathbf{C}_{\mathbf{x},m}(\mathbf{q}_m,\dot{\mathbf{q}}_m)\dot{\mathbf{x}}_m + \mathbf{G}_{\mathbf{x},m}(\mathbf{q}_m) + \mathbf{F}_{\mathbf{x},m}(\dot{\mathbf{q}}_m) = \mathbf{f}_m + \mathbf{f}_{sur} + \mathbf{d}_{\mathbf{x},m} \tag{3}$$

$$\mathbf{M}_{\mathbf{x},s}(\mathbf{q}_s)\ddot{\mathbf{x}}_s + \mathbf{C}_{\mathbf{x},s}(\mathbf{q}_s,\dot{\mathbf{q}}_s)\dot{\mathbf{x}}_s + \mathbf{G}_{\mathbf{x},s}(\mathbf{q}_s) + \mathbf{F}_{\mathbf{x},s}(\dot{\mathbf{q}}_s) = \mathbf{f}_s - \mathbf{f}_{env} + \mathbf{d}_{\mathbf{x},s} \tag{4}$$

where $\mathbf{x}_m$ and $\mathbf{x}_s \in \mathbb{R}^{6\times 1}$ are the Cartesian positions of the master and slave robots' end-effectors, respectively. $\mathbf{f}_m$ and $\mathbf{f}_s \in \mathbb{R}^{6\times 1}$ are the generalized actuator forces of the master and slave robots defined in the Cartesian space, respectively. $\mathbf{f}_{sur}$ and $\mathbf{f}_{env} \in \mathbb{R}^{6\times 1}$ are the interaction forces that the surgeon applies to the master robot and the environment (heart tissue) applies to the slave robot, which are measured by two force sensors attached to the master and slave end-effectors, respectively.

Assumption. It is assumed that the unstructured modeling uncertainties and/or disturbances are bounded and there exist positive constants δ_m and δ_s such that:

$$\left\|\mathbf{d}_{\mathbf{x},m}\right\|_\infty \le \delta_m \ , \quad \left\|\mathbf{d}_{\mathbf{x},s}\right\|_\infty \le \delta_s \tag{5}$$

Using the subscript $i = m$ for the master and $i = s$ for the slave, the matrices of dynamic models in the joint space (Eqs. (1) and (2)) and the Cartesian space (Eqs. (3) and (4)) are related via the non-singular Jacobian matrices $\mathbf{J}_i(\mathbf{q}_i)$ as:

$$\begin{aligned}
&\mathbf{M}_{\mathbf{x},i}(\mathbf{q}_i) = \mathbf{J}_i^{-T}\mathbf{M}_{\mathbf{q},i}(\mathbf{q}_i)\mathbf{J}_i^{-1}, \quad \mathbf{G}_{\mathbf{x},i}(\mathbf{q}_i) = \mathbf{J}_i^{-T}\mathbf{G}_{\mathbf{q},i}(\mathbf{q}_i)\\
&\mathbf{C}_{\mathbf{x},i}(\mathbf{q}_i,\dot{\mathbf{q}}_i) = \mathbf{J}_i^{-T}\left(\mathbf{C}_{\mathbf{q},i}(\mathbf{q}_i,\dot{\mathbf{q}}_i) - \mathbf{M}_{\mathbf{q},i}(\mathbf{q}_i)\mathbf{J}_i^{-1}\dot{\mathbf{J}}_i\right)\mathbf{J}_i^{-1}\\
&\mathbf{F}_{\mathbf{x},i}(\mathbf{q}_i) = \mathbf{J}_i^{-T}\mathbf{F}_{\mathbf{q},i}(\mathbf{q}_i), \quad \mathbf{d}_{\mathbf{x},i} = \mathbf{J}_i^{-T}\mathbf{d}_{\mathbf{q},i}\\
&\mathbf{f}_i = \mathbf{J}_i^{-T}\boldsymbol{\tau}_i \ , \quad \mathbf{f}_{sur} = \mathbf{J}_m^{-T}\boldsymbol{\tau}_{sur} \ , \quad \mathbf{f}_{env} = \mathbf{J}_s^{-T}\boldsymbol{\tau}_{env}
\end{aligned} \tag{6}$$

with the following properties [34-36]:

Property 1. *The left side of Eqs. (1) and (2) can be linearly parameterized as*

$$\mathbf{M}_{\mathbf{q},i}(\mathbf{q}_i)\boldsymbol{\psi}_{\mathbf{1},i}+\mathbf{C}_{\mathbf{q},i}(\mathbf{q}_i,\dot{\mathbf{q}}_i)\boldsymbol{\psi}_{\mathbf{2},i}+\mathbf{G}_{\mathbf{q},i}(\mathbf{q}_i)+\mathbf{F}_{\mathbf{q},i}(\dot{\mathbf{q}}_i) = \mathbf{Y}_{\mathbf{q},i}(\boldsymbol{\psi}_{\mathbf{1},i},\boldsymbol{\psi}_{\mathbf{2},i},\mathbf{q}_i,\dot{\mathbf{q}}_i)\boldsymbol{\beta}_{\mathbf{q},i} \quad (7)$$

where $\boldsymbol{\beta}_{\mathbf{q},i}$ is the vector of unknown parameters of each robot. The regressor matrix $\mathbf{Y}_{\mathbf{q},i}$ includes known functions [34] in terms of the arbitrary vectors $\boldsymbol{\psi}_{\mathbf{1},i}$ and $\boldsymbol{\psi}_{\mathbf{2},i}$.

Property 2. *The matrices* $\left(\dot{\mathbf{M}}_{\mathbf{q},i}(\mathbf{q}_i)-2\mathbf{C}_{\mathbf{q},i}(\mathbf{q}_i,\dot{\mathbf{q}}_i)\right)$ *and* $\left(\dot{\mathbf{M}}_{\mathbf{x},i}(\mathbf{q}_i)-2\mathbf{C}_{\mathbf{x},i}(\mathbf{q}_i,\dot{\mathbf{q}}_i)\right)$ *are skew symmetric.*

3. Impedance Control Objectives for Master-Slave Robotic Surgery of Beating Heart

3.1. Reference Impedance Models for Slave and Master Robots

Two stable reference impedance models are defined and realized for the slave and master robots to perform robotic surgery on beating heart using the proposed bilateral controller.

The reference impedance model of the slave robot is defined as a dynamical relationship between the slave-heart tissue interaction force and the desired slave impedance model's response deviation ($\tilde{\mathbf{x}}_{imp_s}$ in (8)) from the scaled master/surgeon trajectory in Cartesian space as

$$m_s\ddot{\tilde{\mathbf{x}}}_{imp_s}+c_s\dot{\tilde{\mathbf{x}}}_{imp_s}+k_s\tilde{\mathbf{x}}_{imp_s}=-\mathbf{f}_{env} \quad (8)$$

where $\tilde{\mathbf{x}}_{imp_s}=\mathbf{x}_{imp_s}-k_{\mathrm{p}}\mathbf{x}_m$, and k_{p} is the scaling factor for the master/surgeon position. Here, k_s, c_s and m_s are the virtual stiffness, damping and mass parameters of the desired slave impedance model.

The reference impedance model of the master robot is also defined as a dynamics between a summation of the surgeon and scaled heart tissue forces and desired master response trajectory in Cartesian coordinates as

$$m_m\ddot{\mathbf{x}}_{imp_m}+c_m\dot{\mathbf{x}}_{imp_m}+k_m\mathbf{x}_{imp_m}=\mathbf{f}_{sur}-k_{\mathrm{f}}\mathbf{f}_{env} \quad (9)$$

where $\mathbf{x}_{imp_m}$ is the response (position) of the master impedance model. k_{f} is the scaling factor for the slave-heart interaction force. k_m, c_m and m_m are the virtual stiffness, damping and mass parameters of the master impedance model, respectively. As mentioned in Sec. 2, the surgeon ($\mathbf{f}_{sur}$) and the heart tissue ($\mathbf{f}_{env}$) forces are measured by the master and the slave force sensors, respectively, placed at two different points of the tele-robotic system.

The desired responses $\mathbf{x}_{imp_s}$ and $\mathbf{x}_{imp_m}$ of the slave and master impedance models are tracked by the slave and master robots, respectively, using nonlinear robust adaptive control laws presented in Sec. 4. The concepts of two defined stable impedance models (8) and (9) are schematically expressed in Fig. 1. The master impedance model (9) is perceived by the surgeon (as his haptic sense), and the slave impedance model (8) determines the compliance (flexibility) of the slave robot with respect to the surgeon/master trajectory in response to the physiological forces of the heart tissue ($\mathbf{f}_{env}$).

Note that both of the slave (8) and master (9) reference impedance models are stable second-order differential equations when using positive impedance parameters in them.

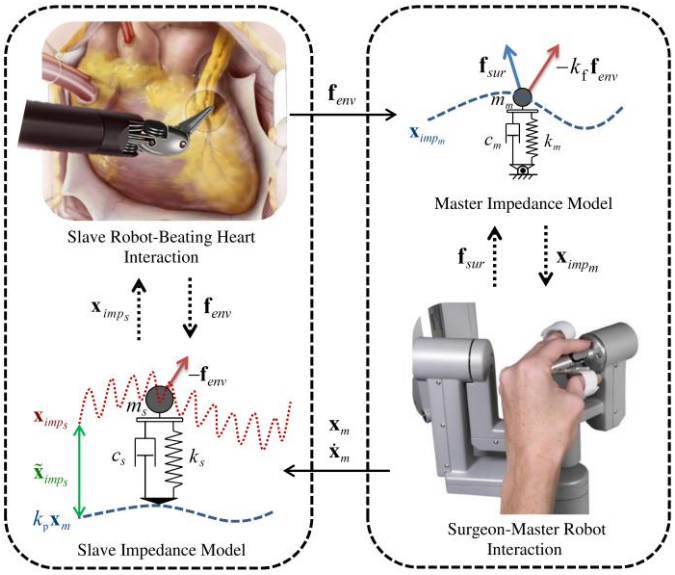

Fig. 1. The concepts of master and slave reference impedance models in the proposed bilateral controller for robotic surgery systems.

3.2. Adjustment of the Slave Impedance Model

The slave impedance model (8) should be adjusted such that the slave robot complies with the physiological force and/or disturbance of the beating heart during the tracking of the scaled master robot's trajectory. For this purpose, using small parameters k_s, c_s and m_s in the slave impedance model (8), the flexibility of the slave robot increases in the sense that it can deviate from the master trajectory ($\tilde{\mathbf{x}}_{imp_s}=\mathbf{x}_{imp_s}-k_{\mathrm{p}}\mathbf{x}_m$) based on the magnitude of the slave-heart interaction force ($\mathbf{f}_{env}$). Therefore, the slave robot end-effector (i.e., surgical tool) will have an oscillatory motion in response to the high-frequency harmonic portion ($\mathbf{f}_{env_{HF}}$) of the heart-robot interaction force $\mathbf{f}_{env}=\mathbf{f}_{env_{HF}}+\mathbf{f}_{env_{LF}}$ originating from the heart's beating motion.

Accordingly, the stiffness value of the slave impedance model (k_s) is designed to have a moderate value based on the desired static relationship between the heart interaction force and the slave robot's deviation from the master trajectory (k_s =

$\mathbf{f}_{env}/\tilde{\mathbf{x}}_{imp_s}$ from Eq. (8) when $\mathbf{f}_{env}$ and consequently $\tilde{\mathbf{x}}_{imp_s}$ are assumed to be constants). It should be noted that too small values of k_s will make the slave robot too flexible such that it cannot apply appropriate forces to the heart tissue. Conversely, too large values of k_s will result a rigid behavior for the slave-tissue interaction such that compliance with the physiological force of the heart is not achieved. This implies a trade-off between the flexibility and the force applying performance of the slave robot.

In addition, the damping ratio of the slave impedance model (8) as a second-order differential equation is set at $\zeta_s = c_s/2\sqrt{m_s k_s} = 0.7$ such that it has a fast behavior in response to the harmonic physiological force of the heart comparing to the dimensionless time $\omega_{n_s} t$ (with appropriate overshoot in response to step forces). Moreover, the natural frequency $\omega_{n_s} = \sqrt{k_s/m_s}$ (which is the cut-off frequency for $\zeta_s = 0.7$) of the slave impedance model (8) should be adjusted larger (e.g., ten times larger) than the range of the heart beating rate ω_{HB}. In other words, the Bode diagram of the slave impedance model (with $\zeta_s = 0.7$) in Fig. 2a shows that if $\omega_{n_s} >> \omega_{HB}$, the $\tilde{\mathbf{x}}_{imp_s}$ (response of (8)) would have its maximum magnitude that is about $\tilde{\mathbf{X}}_{imp_s} = \mathbf{F}_{env}/k_s$. Also, using this frequency adjustment ($\omega_{n_s} > \omega_{HB}$), the desired deviation response ($\tilde{\mathbf{x}}_{imp_s}$) has nearly the same phase as the harmonic physiological force of the heart according to Fig. 2b (i.e., phase distortion does not occur), which is necessary for compliance with the heart's oscillatory motion.

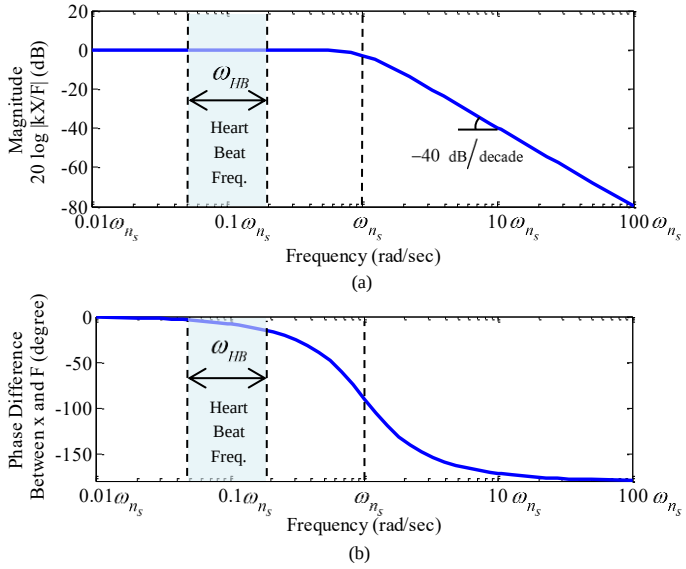

Fig. 2. The Bode diagram of the slave impedance model (with the natural frequency of ω_{n_s} and $\xi_s = 0.7$) for a fast and compliant response to the oscillatory physiological force of the heart (with ω_{HB} frequency): (a) logarithmic magnitude and (b) phase distortion.

Note that if the natural frequency of the slave impedance model (ω_{n_s}) is not adjusted well such that $\omega_{HB} > 0.1\omega_{n_s}$, a phase distortion occurs between the applied oscillatory heart force $\mathbf{f}_{env}$ and the slave deviation response $\tilde{\mathbf{x}}_{imp_s}$. This means that the slave robot will not have an appropriate synchronized flexibility with respect to the heart motion which is undesired for having a persistent interaction with the beating-heart during a surgery operation.

Then, the damping and mass parameters (c_s and m_s) of the slave impedance model (8) are obtained from the above mentioned quantities (k_s, $\zeta_s = c_s/2\sqrt{m_s k_s}$ and $\omega_{n_s} = \sqrt{k_s/m_s}$). The value of position scaling factor in $\tilde{\mathbf{x}}_{imp_s} = \mathbf{x}_{imp_s} - k_p \mathbf{x}_m$ can also be chosen less than one ($k_p < 1$) to enlarge the surgical workspace as much as needed for the surgeon.

3.3. Adjustment of Master Impedance Model

In this bilateral controller, the master impedance model should be designed to provide feedback of the non-oscillatory part of the heart interaction force (like a stationary heart) for the surgeon in the form of force feedback. In the master impedance model (9), employing small values for the parameters k_m, c_m and m_m, the left side of (9) becomes small due to the boundedness of $\mathbf{x}_{imp_m}$, $\dot{\mathbf{x}}_{imp_m}$ and $\ddot{\mathbf{x}}_{imp_m}$. Accordingly, the right side of (9) will be also small ($(\mathbf{f}_{sur} - k_f \mathbf{f}_{env}) \to 0$); therefore, the force reflecting performance is achieved.

However, the high-frequency physiological portion ($\mathbf{f}_{env_{HF}}$) of the total slave-heart interaction force ($\mathbf{f}_{env} = \mathbf{f}_{env_{HF}} + \mathbf{f}_{env_{LF}}$) should not be reflected to the surgeon's hand because it would be challenging and exhausting for the surgeon to perform a surgical operation in the presence of a permanent oscillatory force. To solve this issue using the proposed bilateral controller, the master impedance model (9) are adjusted such that this oscillatory interaction force ($\mathbf{f}_{env_{HF}}$) is filtered and does not affect the desired impedance model's response ($\mathbf{x}_{imp_m}$), which is tracked by the master robot through its nonlinear adaptive controller.

For the purpose of high-frequency force filtration, the second-order master impedance model (9) is designed such that its cut-off frequency ($\approx \omega_n$ for $\zeta_m = c_m/2\sqrt{m_m k_m} = 0.7$) is several times (e.g. ten times) smaller than the beating heart frequency range (ω_{BH}), as shown in Fig. 3.

Similar to the slave impedance model (9) discussed in Sec. 3.2, the damping ratio of the master impedance model (9) is set to $\zeta_m = c_m/2\sqrt{m_m k_m} = 0.7$ in order to have a fast response comparing to the dimensionless time $\omega_{n_m} t$ and appropriate

overshoot.

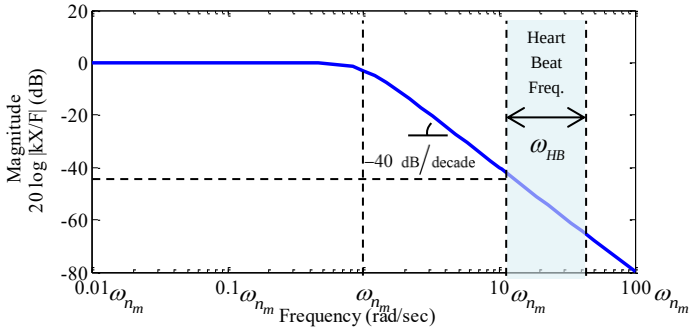

Fig. 3. The Bode diagram of the master impedance model (with the natural frequency of ω_{n_m} and $\xi_m = 0.7$) for filtration of the heart's oscillatory force ($\mathbf{f}_{env_{HF}}$ with ω_{HB} frequency).

The stiffness parameter (k_m) of the master impedance model (9) is chosen small such that the static force reflecting performance ($(\mathbf{f}_{sur} - k_f \mathbf{f}_{env}) \to 0$) is achieved. In other words, when k_m is small, $k_m \mathbf{x}_{imp_m} = \mathbf{f}_{sur} - k_f \mathbf{f}_{env}$ is also small given (9) when $\mathbf{f}_{sur}$, $\mathbf{f}_{env}$ and consequently $\mathbf{x}_{imp_m}$ are considered constant. However, the desired master stiffness (k_m) should not be chosen too small because then the amplitude of the master impedance response to the high-frequency force of the heart would become too large, since $\mathbf{X}_{imp_{m_{HF}}} = -k_f \mathbf{F}_{env_{HF}} / k_m$ based on (9). Therefore, the filtration of this high-frequency force becomes hard and the oscillatory response to this force ($\mathbf{x}_{imp_{m_{HF}}}$) becomes large using too small k_m, which is not desired as discussed above. This trade-off between the force reflection performance and high-frequency force filtration should be considered during the adjustment of k_m.

The damping and mass parameters (c_m and m_m) of the master impedance model are obtained from the above parameters (k_m, $\zeta_m = c_m / 2\sqrt{m_m k_m}$ and $\omega_{n_m} = \sqrt{k_m / m_m}$). Also, the force scaling factor k_f in (9) can be chosen to be more than unity to amplify the applied interaction force of the heart during the surgery for the surgeon. In this case, filtration of the scaled-up oscillatory force of the heart ($k_f \mathbf{f}_{env_{HF}}$) under the surgeon's hand becomes more important.

The normal range of heart beating rate is $\omega_{HB} \simeq 1-1.7$ Hz $= 6.28-10.68$ rad/sec for the above-mentioned adjustments of the slave (8) and master (9) impedance models in Sec. 3.2 and Sec. 3.3, respectively. However, the heart rate of some patients may be lower than the normal range ($\omega_{HB} \simeq 0.4-1$ Hz) or higher than it ($\omega_{HB} \simeq 1.7-3$ Hz), which should be considered in the natural (cut-off) frequency adjustment of the impedance models (Sec. 3.2 and Sec. 3.3).

Due to the sensitivity of robotic surgery on the beating heart, linear reference impedance models (such as (8) and (9)) benefit from their simplicity, stability and possibility of their analysis in the frequency domain. In other words, the specific adjustment of proposed impedance models in Sec. 3.2 and Sec. 3.3 as a contribution of this work on the beating-heart robotic surgery is presented based on the frequency-domain analysis of such linear models. Accordingly, these reference impedance models (8) and (9) are adjusted such that the slave robot has a compliance and agile flexibility in response to the heart interaction force (Sec. 3.2) and the master robot filters the high-frequency portion of this force under the surgeon hand (Sec. 3.3). In addition, the stability of these linear models, input-to-output analysis of them and the provided haptic sense for the surgeon can be appropriately discussed (Sec. 3.1).

4. Nonlinear Bilateral Robust Adaptive Impedance Controller

The responses (positions) of the two reference impedance models (8) and (9) defined in Sec. 3 should be tracked by the slave and master robots, respectively. The dynamic models of multi-DOF master and slave robots are considered to have parametric and bounded non-parametric (unstructured) uncertainties. Therefore, two nonlinear robust adaptive control laws are designed for the master and slave robots in this section. For this purpose, two sliding surfaces are defined for the master and slave controllers as:

$$\begin{aligned} \boldsymbol{\varepsilon}_m &= \dot{\tilde{\mathbf{x}}}_m + \eta_{1,m}\tilde{\mathbf{x}}_m + \eta_{2,m}\int_0^t \tilde{\mathbf{x}}_m \, dt \,, \\ \boldsymbol{\varepsilon}_s &= \dot{\tilde{\mathbf{x}}}_s + \eta_{1,s}\tilde{\mathbf{x}}_s + \eta_{2,s}\int_0^t \tilde{\mathbf{x}}_s \, dt \end{aligned} \tag{10}$$

where $\tilde{\mathbf{x}}_m = \mathbf{x}_m - \mathbf{x}_{imp_m}$ and $\tilde{\mathbf{x}}_s = \mathbf{x}_s - \mathbf{x}_{imp_s}$ are the position tracking errors of the master and slave with respect to the responses of their impedance models (9) and (8), respectively. $\eta_{1,m}$, $\eta_{2,m}$, $\eta_{1,s}$ and $\eta_{2,s}$ are positive constant parameters. Also, the reference velocities are expressed as

$$\begin{aligned} \dot{\mathbf{x}}_{ref,m} &= \dot{\mathbf{x}}_{imp_m} - \eta_{1,m}\tilde{\mathbf{x}}_m - \eta_{2,m}\int_0^t \tilde{\mathbf{x}}_m \, dt \\ \dot{\mathbf{x}}_{ref,s} &= \dot{\mathbf{x}}_{imp_s} - \eta_{1,s}\tilde{\mathbf{x}}_s - \eta_{2,s}\int_0^t \tilde{\mathbf{x}}_s \, dt \end{aligned} \tag{11}$$

such that the sliding surfaces (10) can be represented as $\boldsymbol{\varepsilon}_m = \dot{\mathbf{x}}_m - \dot{\mathbf{x}}_{ref,m}$ and $\boldsymbol{\varepsilon}_s = \dot{\mathbf{x}}_s - \dot{\mathbf{x}}_{ref,s}$. Now, the nonlinear bilateral robust adaptive impedance control (BRAIC) laws for the master and slave end-effectors in Cartesian space are defined as

$$\begin{aligned} \mathbf{f}_m = &-\eta_{3,m}\hat{\mathbf{M}}_{\mathbf{x},m}(\mathbf{q}_m)\boldsymbol{\varepsilon}_m + \hat{\mathbf{M}}_{\mathbf{x},m}(\mathbf{q}_m)\ddot{\mathbf{x}}_{ref,m} \\ &+ \hat{\mathbf{C}}_{\mathbf{x},m}(\mathbf{q}_m,\dot{\mathbf{q}}_m)\dot{\mathbf{x}}_{ref,m} + \hat{\mathbf{G}}_{\mathbf{x},m}(\mathbf{q}_m) + \hat{\mathbf{F}}_{\mathbf{x},m}(\dot{\mathbf{q}}_m) \\ &- \mathbf{f}_{sur} - \hat{\mu}_m \operatorname{sgn}(\boldsymbol{\varepsilon}_m) \end{aligned} \tag{12}$$

$$\begin{aligned}\mathbf{f}_s = &-\eta_{3,s}\,\hat{\mathbf{M}}_{\mathbf{x},s}(\mathbf{q}_s)\boldsymbol{\varepsilon}_s + \hat{\mathbf{M}}_{\mathbf{x},s}(\mathbf{q}_s)\ddot{\mathbf{x}}_{ref,s}\\ &+\hat{\mathbf{C}}_{\mathbf{x},s}(\mathbf{q}_s,\dot{\mathbf{q}}_s)\dot{\mathbf{x}}_{ref,s} + \hat{\mathbf{G}}_{\mathbf{x},s}(\mathbf{q}_s) + \hat{\mathbf{F}}_{\mathbf{x},s}(\dot{\mathbf{q}}_s)\\ &+\mathbf{f}_{env} - \hat{\mu}_s\,\mathrm{sgn}(\boldsymbol{\varepsilon}_s)\end{aligned} \tag{13}$$

The accent $\wedge$ denotes the estimated and/or updated values of matrices, vectors and scalars. It will be proven that the terms $-\hat{\mu}_m\,\mathrm{sgn}(\boldsymbol{\varepsilon}_m)$ and $-\hat{\mu}_s\,\mathrm{sgn}(\boldsymbol{\varepsilon}_s)$ provide the robustness of the bilateral controller against the bounded non-parametric (unstructured) uncertainties. $\hat{\mu}_m$ and $\hat{\mu}_s$ are positive robust gains that are intelligently updated via adaptation laws to overcome the bound of non-parametric uncertainties (as will be presented in the next section). The motor torques of robots (control laws in the joint space) are obtained in terms of joint space matrices and vectors by substituting (6) in (12) and (13) and simplified using Property 1 as

$$\boldsymbol{\tau}_m = \mathbf{Y}_{\mathbf{q},m}\hat{\boldsymbol{\beta}}_{\mathbf{q},m} - \mathbf{J}_m^T\mathbf{f}_{sur} - \mathbf{J}_m^T\hat{\mu}_m\,\mathrm{sgn}(\boldsymbol{\varepsilon}_m) \tag{14}$$

$$\boldsymbol{\tau}_s = \mathbf{Y}_{\mathbf{q},s}\hat{\boldsymbol{\beta}}_{\mathbf{q},s} + \mathbf{J}_s^T\mathbf{f}_{env} - \mathbf{J}_s^T\hat{\mu}_s\,\mathrm{sgn}(\boldsymbol{\varepsilon}_s) \tag{15}$$

where $\mathbf{Y}_{\mathbf{q},m}$ and $\mathbf{Y}_{\mathbf{q},s}$ are obtained from (7) in terms of the following known vectors:

$$\begin{aligned}&\boldsymbol{\psi}_{\mathbf{1},m} = -\eta_{3,m}\mathbf{J}_m^{-1}\boldsymbol{\varepsilon}_m + \mathbf{J}_m^{-1}\ddot{\mathbf{x}}_{ref,m} - \mathbf{J}_m^{-1}\dot{\mathbf{J}}_m\mathbf{J}_m^{-1}\dot{\mathbf{x}}_{ref,m},\\ &\boldsymbol{\psi}_{\mathbf{1},s} = -\eta_{3,s}\mathbf{J}_s^{-1}\boldsymbol{\varepsilon}_s + \mathbf{J}_s^{-1}\ddot{\mathbf{x}}_{ref,s} - \mathbf{J}_s^{-1}\dot{\mathbf{J}}_s\mathbf{J}_s^{-1}\dot{\mathbf{x}}_{ref,s},\\ &\boldsymbol{\psi}_{\mathbf{2},m} = \mathbf{J}_m^{-1}\dot{\mathbf{x}}_{ref,m}\ ,\quad \boldsymbol{\psi}_{\mathbf{2},s} = \mathbf{J}_s^{-1}\dot{\mathbf{x}}_{ref,s}\end{aligned} \tag{16}$$

To obtain the closed-loop dynamics of the master and slave robots using the presented nonlinear bilateral controller, the control laws (12) and (13) are substituted in the end-effector dynamics (3) and (4) of the tele-robotic system, which turn out after some simplifications as

$$\begin{aligned}&\mathbf{M}_{\mathbf{x},m}(\dot{\boldsymbol{\varepsilon}}_m + \eta_{3,m}\boldsymbol{\varepsilon}_m) + \mathbf{C}_{\mathbf{x},m}\boldsymbol{\varepsilon}_m =\\ &\qquad + \mathbf{J}_m^{-T}\mathbf{Y}_{\mathbf{q},m}\tilde{\boldsymbol{\beta}}_{\mathbf{q},m} + \mathbf{d}_{\mathbf{x},m} - \hat{\mu}_m\,\mathrm{sgn}(\boldsymbol{\varepsilon}_m)\end{aligned} \tag{17}$$

$$\begin{aligned}&\mathbf{M}_{\mathbf{x},s}(\dot{\boldsymbol{\varepsilon}}_s + \eta_{3,s}\boldsymbol{\varepsilon}_s) + \mathbf{C}_{\mathbf{x},s}\boldsymbol{\varepsilon}_s =\\ &\qquad + \mathbf{J}_s^{-T}\mathbf{Y}_{\mathbf{q},s}\tilde{\boldsymbol{\beta}}_{\mathbf{q},s} + \mathbf{d}_{\mathbf{x},s} - \hat{\mu}_s\,\mathrm{sgn}(\boldsymbol{\varepsilon}_s)\end{aligned} \tag{18}$$

where $\tilde{\boldsymbol{\beta}}_{\mathbf{q},m} = \hat{\boldsymbol{\beta}}_{\mathbf{q},m} - \boldsymbol{\beta}_{\mathbf{q},m}$ and $\tilde{\boldsymbol{\beta}}_{\mathbf{q},s} = \hat{\boldsymbol{\beta}}_{\mathbf{q},s} - \boldsymbol{\beta}_{\mathbf{q},s}$ are the estimation errors of master and slave dynamic parameters, respectively.

5. Lyapunov Stability Proof and Adaptation Laws

In this section, the stability of the proposed controlled tele-robotic system and tracking convergence of the robots' trajectories to desired impedance responses ($\mathbf{x}_m \to \mathbf{x}_{imp_m}$ and $\mathbf{x}_s \to \mathbf{x}_{imp_s}$) are proven. Also, the robustness of proposed controller against parametric and bounded non-parametric uncertainties is guaranteed via two adaptation laws. For these purposes, a positive definite Lyapunov function is defined as

$$\begin{aligned}V(t) = \frac{1}{2}\big(&\boldsymbol{\varepsilon}_m^T\mathbf{M}_{\mathbf{x},m}\boldsymbol{\varepsilon}_m + \tilde{\boldsymbol{\beta}}_{\mathbf{q},m}^T\mathbf{H}_m^{-1}\tilde{\boldsymbol{\beta}}_{\mathbf{q},m} + (1/\gamma_m)(\hat{\mu}_m - \delta_m)^2\\ &+\boldsymbol{\varepsilon}_s^T\mathbf{M}_{\mathbf{x},s}\boldsymbol{\varepsilon}_s + \tilde{\boldsymbol{\beta}}_{\mathbf{q},s}^T\mathbf{H}_s^{-1}\tilde{\boldsymbol{\beta}}_{\mathbf{q},s} + (1/\gamma_s)(\hat{\mu}_s - \delta_s)^2\big)\end{aligned} \tag{19}$$

where δ_m and δ_s are the unknown upper bounds of the unstructured (non-parametric) modeling uncertainties, introduced in (5). $\mathbf{H}_m$ and $\mathbf{H}_s$ are symmetric positive-definite matrices. γ_m and γ_s are also positive constants.

Now, the time derivative of the Lyapunov function (19) is obtained as

$$\begin{aligned}\dot{V}(t) = &(1/2)\boldsymbol{\varepsilon}_m^T\dot{\mathbf{M}}_{\mathbf{x},m}\boldsymbol{\varepsilon}_m + \boldsymbol{\varepsilon}_m^T\mathbf{M}_{\mathbf{x},m}\dot{\boldsymbol{\varepsilon}}_m\\ &+\dot{\tilde{\boldsymbol{\beta}}}_{\mathbf{q},m}^T\mathbf{H}_m^{-1}\tilde{\boldsymbol{\beta}}_{\mathbf{q},m} + (1/\gamma_m)(\hat{\mu}_m - \delta_m)\dot{\hat{\mu}}_m\\ &+(1/2)\boldsymbol{\varepsilon}_s^T\dot{\mathbf{M}}_{\mathbf{x},s}\boldsymbol{\varepsilon}_s + \boldsymbol{\varepsilon}_s^T\mathbf{M}_{\mathbf{x},s}\dot{\boldsymbol{\varepsilon}}_s\\ &+\dot{\tilde{\boldsymbol{\beta}}}_{\mathbf{q},s}^T\mathbf{H}_s^{-1}\tilde{\boldsymbol{\beta}}_{\mathbf{q},s} + (1/\gamma_s)(\hat{\mu}_s - \delta_s)\dot{\hat{\mu}}_s\end{aligned} \tag{20}$$

where $\dot{\tilde{\boldsymbol{\beta}}}_{\mathbf{q},i} = \dot{\hat{\boldsymbol{\beta}}}_{\mathbf{q},i}$ because $\tilde{\boldsymbol{\beta}}_{\mathbf{q},i} = \hat{\boldsymbol{\beta}}_{\mathbf{q},i} - \boldsymbol{\beta}_{\mathbf{q},i}$ and the actual parameters are constant ($\dot{\boldsymbol{\beta}}_{\mathbf{q},i} = 0$). Employing $\mathbf{M}_{\mathbf{x},m}\dot{\boldsymbol{\varepsilon}}_m$ and $\mathbf{M}_{\mathbf{x},s}\dot{\boldsymbol{\varepsilon}}_s$ from (17) and (18) and according to Property 2 of robot manipulator dynamics ($\dot{\mathbf{M}}_{\mathbf{x},i} - 2\mathbf{C}_{\mathbf{x},i}$ is skew symmetric), Eq. (20) is found as

$$\begin{aligned}\dot{V}(t) = &-\eta_{3,m}\boldsymbol{\varepsilon}_m^T\mathbf{M}_{\mathbf{x},m}\boldsymbol{\varepsilon}_m + \boldsymbol{\varepsilon}_m^T\mathbf{J}_m^{-T}\mathbf{Y}_{\mathbf{q},m}\tilde{\boldsymbol{\beta}}_{\mathbf{q},m} + \dot{\tilde{\boldsymbol{\beta}}}_{\mathbf{q},m}^T\mathbf{H}_m^{-1}\tilde{\boldsymbol{\beta}}_{\mathbf{q},m}\\ &+\boldsymbol{\varepsilon}_m^T(\mathbf{d}_{\mathbf{x},m} - \hat{\mu}_m\,\mathrm{sgn}(\boldsymbol{\varepsilon}_m)) + (1/\gamma_m)(\hat{\mu}_m - \delta_m)\dot{\hat{\mu}}_m\\ &-\eta_{3,s}\boldsymbol{\varepsilon}_s^T\mathbf{M}_{\mathbf{x},s}\boldsymbol{\varepsilon}_s + \boldsymbol{\varepsilon}_s^T\mathbf{J}_s^{-T}\mathbf{Y}_{\mathbf{q},s}\tilde{\boldsymbol{\beta}}_{\mathbf{q},s} + \dot{\tilde{\boldsymbol{\beta}}}_{\mathbf{q},s}^T\mathbf{H}_s^{-1}\tilde{\boldsymbol{\beta}}_{\mathbf{q},s}\\ &+\boldsymbol{\varepsilon}_s^T(\mathbf{d}_{\mathbf{x},s} - \hat{\mu}_s\,\mathrm{sgn}(\boldsymbol{\varepsilon}_s)) + (1/\gamma_s)(\hat{\mu}_s - \delta_s)\dot{\hat{\mu}}_s\end{aligned} \tag{21}$$

Now, the first adaptation law for updating the estimated parameters of the robotic surgery system is expressed as

$$\dot{\hat{\boldsymbol{\beta}}}_{\mathbf{q},m} = -\mathbf{H}_m^T\,\mathbf{Y}_{\mathbf{q},m}^T\,\mathbf{J}_m^{-1}\boldsymbol{\varepsilon}_m\ ,\quad \dot{\hat{\boldsymbol{\beta}}}_{\mathbf{q},s} = -\mathbf{H}_s^T\,\mathbf{Y}_{\mathbf{q},s}^T\,\mathbf{J}_s^{-1}\boldsymbol{\varepsilon}_s \tag{22}$$

such that the terms in (21) including $\tilde{\boldsymbol{\beta}}_{\mathbf{q},m}$ and $\tilde{\boldsymbol{\beta}}_{\mathbf{q},s}$ are cancelled, i.e., the adaptive controller becomes robust against parametric uncertainties. Then, having $\boldsymbol{\varepsilon}_i^T\,\mathrm{sgn}(\boldsymbol{\varepsilon}_i) = \|\boldsymbol{\varepsilon}_i\|_1$, we get

$$\begin{aligned}\dot{V}(t) = &-\eta_{3,m}\boldsymbol{\varepsilon}_m^T\mathbf{M}_{\mathbf{x},m}\boldsymbol{\varepsilon}_m + \boldsymbol{\varepsilon}_m^T\mathbf{d}_{\mathbf{x},m} - \hat{\mu}_m\|\boldsymbol{\varepsilon}_m\|_1\\ &+(1/\gamma_m)(\hat{\mu}_m - \delta_m)\dot{\hat{\mu}}_m\\ &-\eta_{3,s}\boldsymbol{\varepsilon}_s^T\mathbf{M}_{\mathbf{x},s}\boldsymbol{\varepsilon}_s + \boldsymbol{\varepsilon}_s^T\mathbf{d}_{\mathbf{x},s} - \hat{\mu}_s\|\boldsymbol{\varepsilon}_s\|_1\\ &+(1/\gamma_s)(\hat{\mu}_s - \delta_s)\dot{\hat{\mu}}_s\end{aligned} \tag{23}$$

The second adaptation law for updating the robust gains $\hat{\mu}_m$ and $\hat{\mu}_s$ of the controller (12) and (13) is defined as

$$\begin{aligned}&\dot{\hat{\mu}}_m = \gamma_m\|\boldsymbol{\varepsilon}_m\|_1\ ,\quad \hat{\mu}_m(0) = \hat{\mu}_{m0} > 0\\ &\dot{\hat{\mu}}_s = \gamma_s\|\boldsymbol{\varepsilon}_s\|_1\ ,\quad \hat{\mu}_s(0) = \hat{\mu}_{s0} > 0\end{aligned} \tag{24}$$

where $\hat{\mu}_{m0}$ and $\hat{\mu}_{s0}$ are positive constants being the initial values of the robust gains at $t = 0$. Using the above-mentioned adaptation laws (24), Eq. (23) is simplified as

$$\dot{V}(t) = \boldsymbol{\varepsilon}_m^T \mathbf{d}_{\mathbf{x},m} - \delta_m \left\| \boldsymbol{\varepsilon}_m \right\|_1 - \eta_{3,m} \boldsymbol{\varepsilon}_m^T \mathbf{M}_{\mathbf{x},m} \boldsymbol{\varepsilon}_m + \boldsymbol{\varepsilon}_s^T \mathbf{d}_{\mathbf{x},s} - \delta_s \left\| \boldsymbol{\varepsilon}_s \right\|_1 - \eta_{3,s} \boldsymbol{\varepsilon}_s^T \mathbf{M}_{\mathbf{x},s} \boldsymbol{\varepsilon}_s \quad (25)$$

Due to the boundedness condition of the unstructured non-parametric uncertainties ($\mathbf{d}_{\mathbf{x},m}$ and $\mathbf{d}_{\mathbf{x},s}$) presented in (5), the time derivative of Lyapunov function is finally obtained as

$$\dot{V}(t) \le -\eta_{3,m} \boldsymbol{\varepsilon}_m^T \mathbf{M}_{\mathbf{x},m} \boldsymbol{\varepsilon}_m - \eta_{3,s} \boldsymbol{\varepsilon}_s^T \mathbf{M}_{\mathbf{x},s} \boldsymbol{\varepsilon}_s \quad (26)$$

Since the Lyapunov function (19) is positive definite ($V(t) > 0$) and its time derivative (26) is negative semi-definite ($\dot{V}(t) \le 0$), $V(t)$ is bounded. As a result, the boundedness of $\boldsymbol{\varepsilon}_m$, $\boldsymbol{\varepsilon}_s$, $\tilde{\boldsymbol{\beta}}_{\mathbf{q},m}$, $\tilde{\boldsymbol{\beta}}_{\mathbf{q},s}$, $(\hat{\mu}_m - \delta_m)$ and $(\hat{\mu}_s - \delta_s)$ is concluded considering (19). Moreover, it is proven using the Barbalat's lemma [34] that $\dot{V}(t) \to 0$ as $t \to \infty$. Since $\eta_{3,m} > 0$, $\eta_{3,s} > 0$, $\boldsymbol{\varepsilon}_m^T \mathbf{M}_{\mathbf{x},m} \boldsymbol{\varepsilon}_m \ge 0$ and $\boldsymbol{\varepsilon}_s^T \mathbf{M}_{\mathbf{x},s} \boldsymbol{\varepsilon}_s \ge 0$, $\dot{V}(t) \to 0$ imply the convergence to sliding surfaces $\boldsymbol{\varepsilon}_m = 0$ and $\boldsymbol{\varepsilon}_s = 0$ as $t \to \infty$. Thus, according to the stable dynamics of the sliding surfaces $\boldsymbol{\varepsilon}_m$ and $\boldsymbol{\varepsilon}_s$ in (10), the convergence of the master and slave tracking errors to zero $\tilde{\mathbf{x}}_m \to 0$ (i.e., $\mathbf{x}_m \to \mathbf{x}_{imp_m}$) and $\tilde{\mathbf{x}}_s \to 0$ (i.e., $\mathbf{x}_s \to \mathbf{x}_{imp_s}$) on the surfaces of $\boldsymbol{\varepsilon}_m = 0$ and $\boldsymbol{\varepsilon}_s = 0$ are established.

6. Experiments

The bilateral impedance controller is evaluated experimentally in this section to show its performance for the robotic surgery on a simulated beating heart. In the designed experiments, the Phantom Premium 1.5A robot (Geomagic Inc., Wilmington, MA, USA) with three DOFs and the Quanser robot (Quanser Consulting Inc., Markham, ON, Canada) with two DOFs are employed as the master and slave robots (Fig. 4). To measure the applied interaction forces of the surgeon (human operator) and the heart tissue, the Phantom Premium and Quanser robots are respectively equipped with a 6-axis 50M31 force/torque sensor (JR3 Inc., Woodland, CA, USA) and a 6-axis Gamma force/torque sensor (ATI Industrial Automation, Apex, NC, USA). The slave (Quanser) robot is equipped with a stapling device to mimic a realistic surgical task in mitral valve annuloplasty. This surgery is used for implanting an annuloplasty ring onto the mitral valve using several staples in order to reshape this valve during the normal beating motion of the heart. Note that the human operator (shown in Fig. 4) only applies the force $\mathbf{f}_{sur}$ to the master robot during the experiment. He also clicks a button at the end of flexible cable of the stapling device by his other hand in this experimental set-up, without applying any force to the slave robot. Accordingly, the slave force sensor purely measures the heart-tissue interaction force $\mathbf{f}_{env}$ as expected and required in the presented impedance models (8) and (9) of this strategy (Sec. 3).

In addition, a beating heart motion simulator device is utilized to replicate the physiological motion of the mitral valve annulus. It should be mentioned that although the mitral valve has 3D movements, the motion of the mitral valve annulus, onto which the annuloplasty ring needs to be sutured, is mostly one directional [7, 31, 32] as was shown in 3D ultrasound (US) images [37] and simulated in these experiments. An artificial soft tissue is also attached to this device as shown in Fig. 4. Note that a healthy human operator behaves as the surgeon in these experiments.

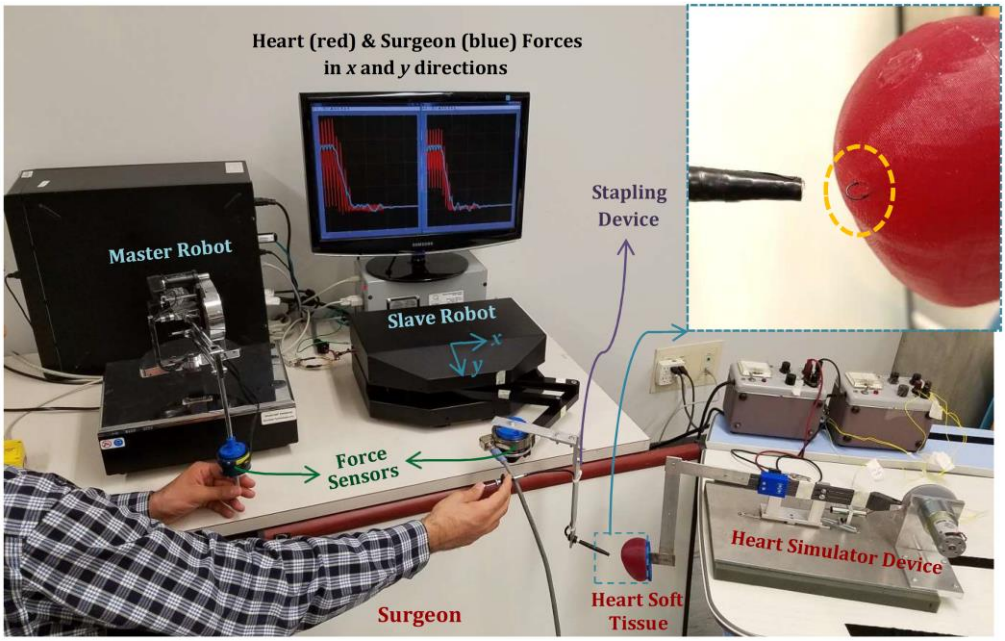

Fig. 4. The experimental system for robotic surgery with application in the mitral valve annuloplasty of the beating heart, including the master and slave robots and their accessories in addition to the heart simulator device. The monitor shows the on-line surgeon-master and slave-heart interaction forces in *x* and *y* directions.

The QUARC software (Quanser Consulting Inc., Markham, ON, Canada) is used as a real-time control environment to implement the proposed bilateral impedance controller with a sampling rate of $1\ k\text{Hz}$.

The workspace of the slave (Quanser) robot is a subset of $x-y$ plane and the master (Phantom) robot is controlled to move in the same 2D space as shown in Fig. 4. The kinematics and dynamics of the Phantom Premium and Quanser robots were comprehensively presented in [38] and [39, 40], respectively, and are not presented here for the sake of brevity. The "sgn($\boldsymbol{\varepsilon}_i$)" function in the control laws (12) and (13) leads to undesired discontinuities and chattering in the input torques. Therefore, the "sgn($\boldsymbol{\varepsilon}_i$)" function is replaced in practice by the continuous approximation $\tanh(150\boldsymbol{\varepsilon}_i)$, where $\boldsymbol{\varepsilon}_i$ is defined in Eq. (10) for the master ($i=m$) and the slave ($i=s$).

The heart rate in the experiments presented in the following Sec. 6.1, 6.2 and 6.3 is 70 beats/min which is in the normal range $\omega_{HB} \simeq 60-100$ beats/min $=1-1.7$ Hz for adults.

6.1. Appropriate Adjustments of Impedance Models

The parameters of the slave (8) and the master (9) impedance models are chosen according to the adjustment procedures discussed in Sec. 3.2 and 3.3, respectively, and listed in Table 1. Note that these parameters are scalar; however, without loss of generality, they can be set to be diagonal matrices with different element values in order to have various characteristics in different directions of Cartesian space.

Table 1. Parameters of the master and slave impedance models for robotic surgery of normal beating heart $\omega_{HB} \simeq 60-100$ beats/min

Master impedance parameters	Slave impedance parameters	Force and position scaling factors
$k_m = 4$ N/m	$k_s = 100$ N/m	$k_{\text{f}} = 2$
$c_m = 11.2$ N.s/m	$c_s = 2.8$ N.s/m	$k_{\text{p}} = 0.7$
$m_m = 16$ kg	$m_s = 0.04$ kg	

As seen in Fig. 5, the master and slave robots' end-effectors track their corresponding impedance responses in the x and y directions during the entire operation using the proposed bilateral adaptive controller.

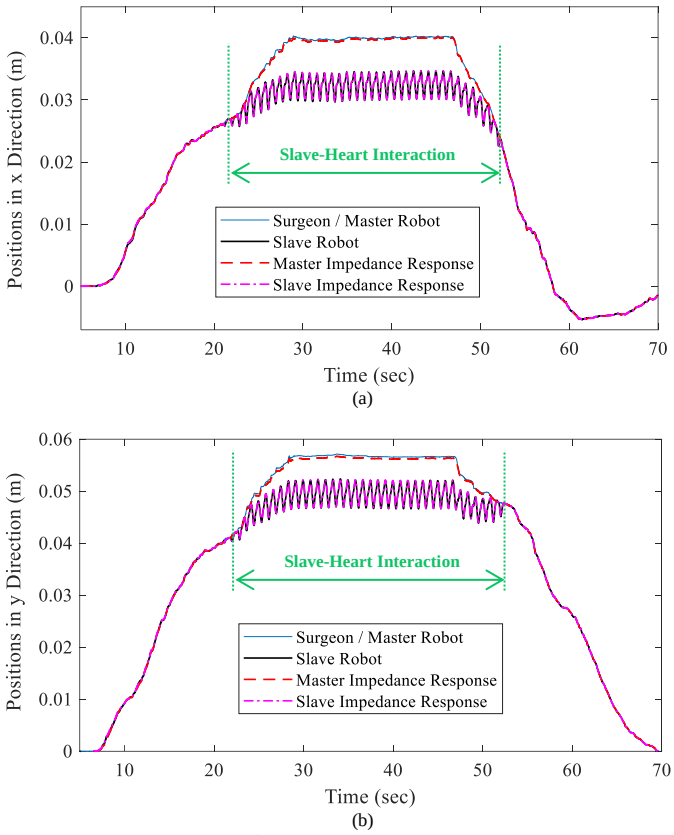

Fig. 5. Position trajectories of the master and slave robots track their respective impedance models responses, in (a) x and (b) y directions.

However, based on the slave impedance model (8), after starting the heart interaction and applying the heart force $\mathbf{f}_{env}$ to the slave robot, the slave has some flexibility and deviation $\tilde{\mathbf{x}}_{imp_s}$ from the master trajectory in Fig. 5. Therefore, the slave robot has a fast compliant response based on the applied interaction force $\mathbf{f}_{env}$ and adjusted characteristics of the impedance model (8).

The scaled-up applied interaction force between the heart tissue and the slave robot ($k_{\text{f}}\mathbf{f}_{env}$) together with the applied interaction force from the operator/surgeon to the master robot ($\mathbf{f}_{sur}$) in the x and y directions are plotted in Fig. 6. As it is observed in Fig. 6, the surgeon applies a force to move the master and consequently the slave robots when the tissue environment force $\mathbf{f}_{env}$ is zero. After starting the interaction, the oscillatory component of the force of the beating heart is applied to the slave and causes the deviation of the slave trajectory from the master one (as shown in Fig. 5). Based on Fig. 6, the operator/surgeon perceives the non-oscillatory (low-frequency) portion $k_{\text{f}}\mathbf{f}_{env_{LF}}$ of the slave-heart interaction force in the form of haptic feedback, which is the result of master impedance model (9) adjustment. According to this force reflection performance (Fig. 6), the operator's sense is made similar to that experienced in a stopped-heart surgery.

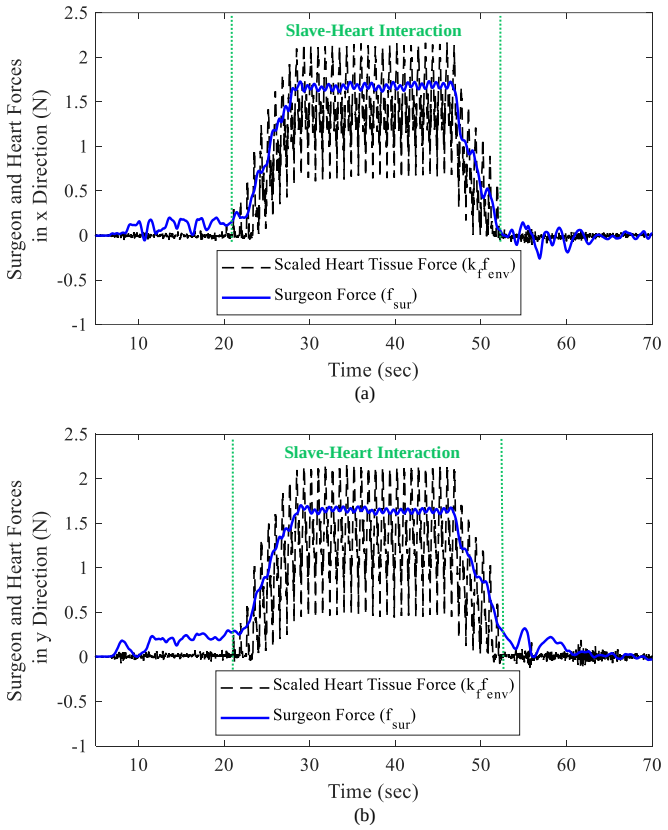

Fig. 6. Scaled-up heart force (with $k_f = 2$) and the surgeon's force applied, respectively, to the slave and master robots, in (a) x and (b) y directions.

To elaborate more on the performance of the bilateral adaptive controller, Fig. 7 shows the convergence of robots trajectories to sliding surfaces $\boldsymbol{\varepsilon}_m = 0$ and $\boldsymbol{\varepsilon}_s = 0$, which is consistent with the Lyapunov stability proof (Sec. 5). Moreover, since the robots have zero initial errors with respect to their impedance models' responses, the tracking errors remain small even before the convergence to zero (Fig. 7). Note that the chattering of errors around the sliding surfaces ($\boldsymbol{\varepsilon}_m = 0$ and $\boldsymbol{\varepsilon}_s = 0$) is prevented by employing the continuous function $\tanh(150\boldsymbol{\varepsilon}_i)$ instead of $\text{sgn}(\boldsymbol{\varepsilon}_i)$ in implementation of the control laws (12) and (13).

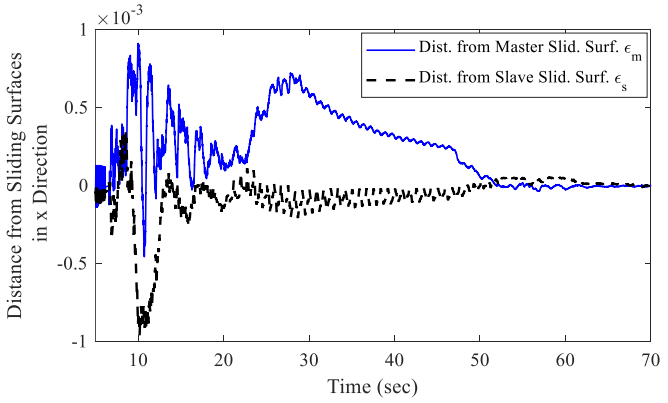

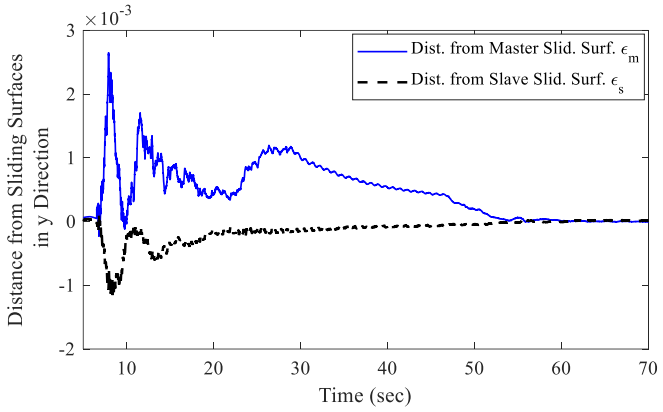

Fig. 7. Distance from the master and the slave sliding surfaces ($\boldsymbol{\varepsilon}_m$ and $\boldsymbol{\varepsilon}_s$).

As seen in Figs. 5 and 6, the control objectives that are (1) the slave robot's flexibility (deviation from the master trajectory) during the interaction with the heart, and (2) the reflection of non-oscillatory force of the heart to the operator are achieved.

Figure 8 shows the performance of the second adaptation law (24) in updating the robust gains $\hat{\mu}_m$ and $\hat{\mu}_s$ of the controller to provide robustness against bounded unstructured uncertainties as proven in Sec. 5. As seen, these robust gains increase as much as needed to overcome uncertainties and finally converge to constant values ($\dot{\hat{\mu}}_m \to 0$ and $\dot{\hat{\mu}}_s \to 0$) based on Eq. (24) as a result of convergence to sliding surfaces $\boldsymbol{\varepsilon}_m \to 0$ and $\boldsymbol{\varepsilon}_s \to 0$ (shown in Fig. 7). Accordingly, the upper bounds of master and slave robots' disturbances (δ_m and δ_s in Eq. (5)) can be estimated less than 1 N due to the final values of robust gains $\hat{\mu}_m$ and $\hat{\mu}_s$ in Fig. 8, as discussed in Sec. 5.

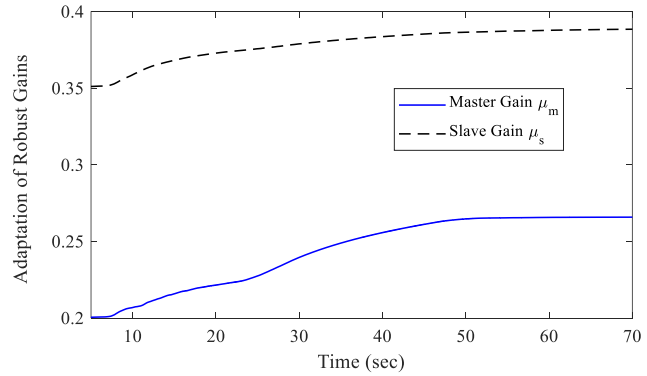

Fig. 8. The update process of robust gains $\hat{\mu}_m$ and $\hat{\mu}_s$ in the bilateral controller using the second adaptation law (24).

6.2. Inappropriate Adjustments of Impedance Models

In this section, the experimental results for two cases of inappropriate adjustment of the impedance models are shown. In the first case, the natural (or cut-off) frequency ω_{n_s} of the slave impedance model (8) is chosen $\omega_{n_s} = \sqrt{k_s/m_s}$

$= 2$ rad/sec to be less than the frequency of the heart beat ($\omega_{HB} \simeq 6.28 - 10.68$ rad/sec). Accordingly, using the same slave impedance model's stiffness and damping ratio as in the previous section ($k_s = 100$ N/m and $\zeta_s = c_s / 2\sqrt{m_s k_s} = 0.7$), only the damping and mass parameters of the slave impedance model in Table 1 change to $c_s = 70$ N.s/m and $m_s = 25$ kg, respectively. As observed in Fig. 9a, the slave robot becomes too sluggish and cannot comply with the beating heart oscillatory motions unlike the previous case in Sec. 6.1 (Fig. 5) which has the appropriate adjustment with a large ω_{n_s}. Due to this slow and rigid behavior of the reference slave impedance model, the slave robot-heart interaction force ($\mathbf{f}_{env}$ in Fig. 9b) becomes too large (more than 5 N) during the oscillatory motions of the heart, which is dangerous for the heart's delicate tissue.

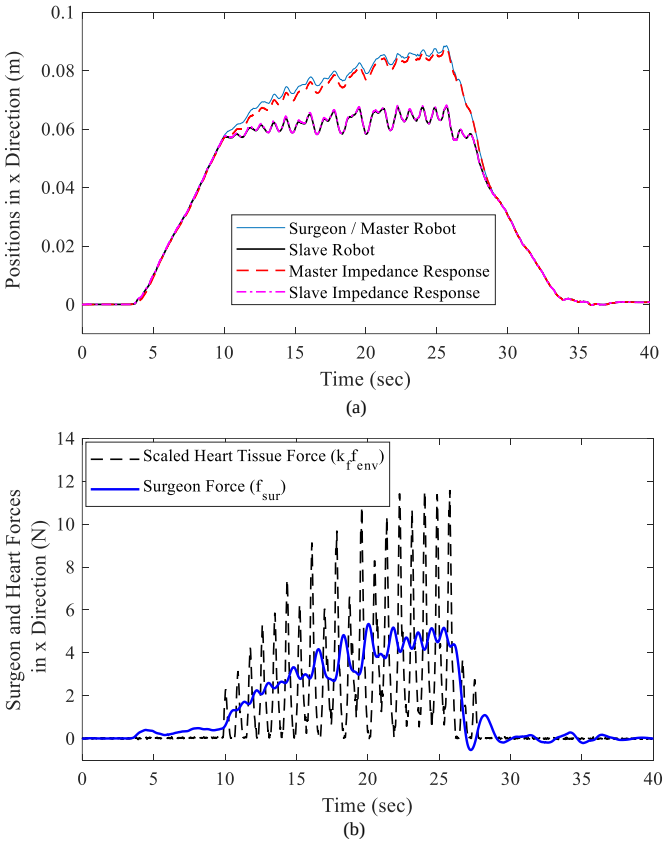

Fig. 9. (a) Position trajectories and (b) interaction forces, when the slave impedance is not adjusted appropriately to have an agile yet compliant response in response to the heart interaction forces.

In the next case of inappropriate adjustment, the master stiffness is considered to be $k_m = 1$, which is four times smaller than the appropriate value used in Sec. 6.1. The other parameters of the master impedance model (9) are obtained as $c_m = 2.8$ N.s/m and $m_m = 4$ kg using the same natural frequency $\omega_{n_m} = 0.5$ rad/sec and the damping ratio $\zeta_m = 0.7$ as ones employed in Sec. 6.1. The other parameters are the same as ones presented in Table 1.

According to Fig. 10, the scaled-up oscillatory force component $k_f \mathbf{f}_{env_{HF}}$ of the beating heart (with $k_f = 2$) is not filtered out and is instead reflected to the operator via the master robot. In this case, the operator should try to overcome these high-frequency forces via $\mathbf{f}_{sur}$ (Fig. 10b) in order to maintain a desired position (Fig. 10a). This performance comes from too small value of the master impedance model stiffness k_m that increases amplitude of the master impedance response to the high-frequency component of the heart force $\mathbf{x}_{imp_{m_{HF}}} = -k_f \mathbf{F}_{env_{HF}} / k_m$ as discussed in Sec. 3.3.

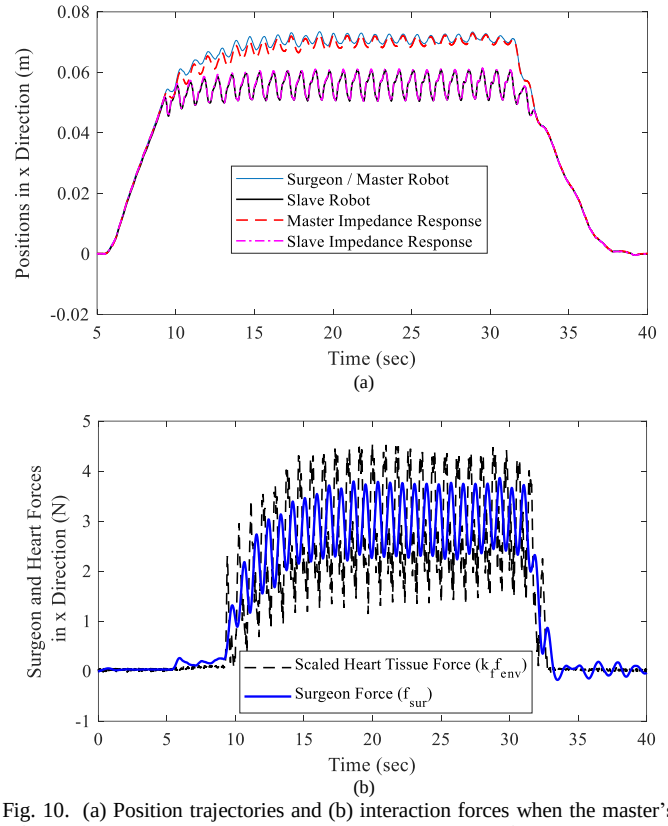

Fig. 10. (a) Position trajectories and (b) interaction forces when the master's reference impedance model is not adjusted appropriately to filter the oscillatory portion of the heart interaction forces.

6.3. Evaluation of Direct Force Reflection (DFR) Strategy

For the purpose of comparison, performance of the DFR control method [11] is evaluated in the same surgical task (stapling with application in mitral valve annuloplasty).

As seen in Fig. 11, the DFR strategy is provided position and force tracking performances without having any position flexibility and high-frequency force filtration between the master and slave robots. Therefore, the operator/surgeon should compensate the oscillatory motion of the beating-heart manually by trying to have the same motion in his hand (master end-effector), as shown in Fig. 11. However, the operator could not have a persistent oscillatory motion like the heart, which results in detachment form the heart tissue surface and/or pressing it more than enough in some moments (causes sudden large forces). Accordingly, the DFR control method [11] makes

the beating-heart surgery hard such that the surgeon should concentrate on the motion compensation in addition to the surgery task.

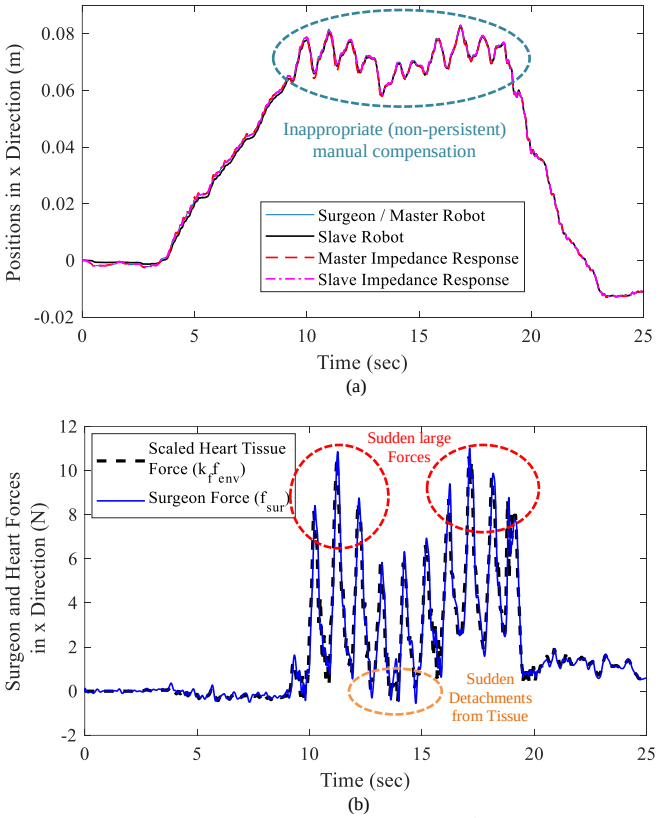

Fig. 11. (a) Position trajectories and (b) interaction forces, when the DFR control strategy [11] is implemented and the manual compensation is required.

6.4. Evaluation of the Proposed Strategy in High Heart Rates

In this section, the proposed impedance-based bilateral controller is evaluated experimentally for high rates of the heart beat ($\omega_{HB} \simeq 100-180$ beats/min $=1.7-3$ Hz). For this case, parameters of the impedance models (8) and (9) are adjusted based on procedures presented in Sec. 3.2 and 3.3 and expressed in Table 2, where the same stiffness parameters (k_m and k_s) as ones in Sec. 6.1 (Table 1) are used.

Table 2. Parameters of the impedance models for robotic surgery of beating heart with high beat rates $\omega_{HB} \simeq 100-180$ beats/min

Master impedance parameters	Slave impedance parameters	Force and position scaling factors
$k_m = 4$ N/m	$k_s = 100$ N/m	$k_f = 2$
$c_m = 5.6$ N.s/m	$c_s = 0.467$ N.s/m	$k_p = 0.7$
$m_m = 4$ kg	$m_s = 0.011$ kg	

Figure 12 illustrates that the master and slave robots could provide the desired position flexibility (Fig. 12a) and force filtration (Fig. 12b) by appropriate tracking of their reference impedance responses with the heart-beat rate of $\omega_{HB} \simeq 150$ beats/min .

Note that performance of the DFR strategy in this case (high heart rate) is not shown here for the sake of brevity. However, it will be worse than the presented one in Sec. 6.3 for the normal heart rate $\omega_{HB} \simeq 70$ beats/min , which is because that the manual compensation of heart's oscillatory motion becomes harder for the operator in higher heart rates (e.g., $\omega_{HB} \simeq 150$ beats/min).

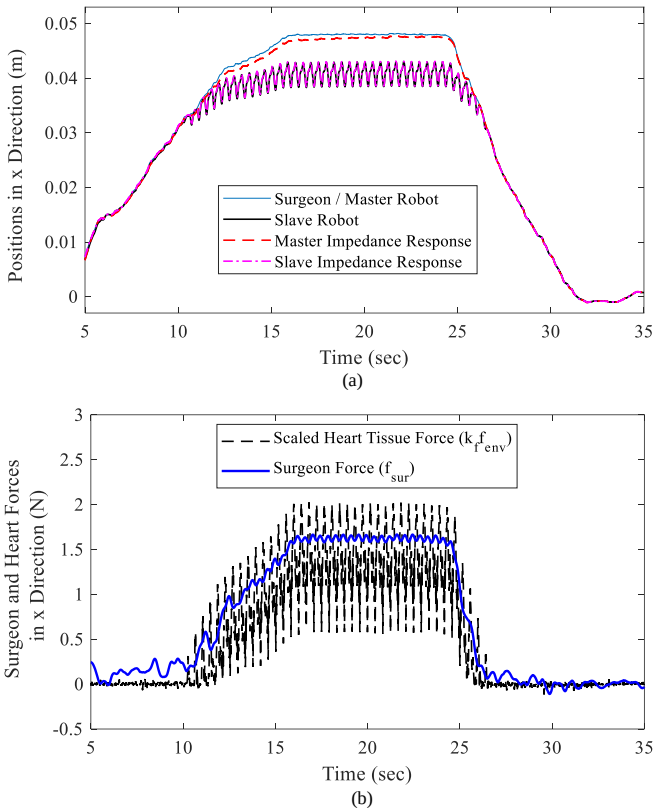

Fig. 12. (a) Position trajectories and (b) interaction forces using the proposed controller for a high heart beat rate $\omega_{HB} \simeq 150$ beats/min .

It should be mentioned that the maximum admissible position tracking error during a beating-heart operation depends on the rigidity of the surgical tool and the specific task objective. For precise positioning tasks, 1-2 mm of position error is admissible. In cases where the tool is soft or the task requires force or impedance control with a flexible tool-tissue interaction rather than position control (e.g., using a catheter for heart tissue ablation), position errors can be larger.

In the conducted experiments (shown in Figs. 5, 9a, 10a and 12a), the slave and master tracking errors are less than 2 mm, which are acceptable in the proposed impedance control strategy for the beating-heart robotic surgery.

6.5. Technical Notes

6.5.1. Implications for Low Beating Rate

In some patients (e.g., having Bradycardia) that their heart

rates are lower than the normal range ($\omega_{HB} < 1$ Hz $= 6.28$ rad/sec), the natural (cut-off) frequency of the master impedance model (ω_{n_m}) should be decreased for filtration of high-frequency force of the heart, as discussed in Sec. 3.3. Consequently, the master impedance parameters should be changed in comparison with the values presented in Table 1.

Note that the proposed robotic surgery is evaluated for moderate and high heart rates in Sec. 6.1 and Sec. 6.4, respectively. Different adjustments of master impedance parameters are mentioned in Table 1 and Table 2 in order to filter high-frequency force of the heart under the surgeon hand.

6.5.2. Existence of Trocar Friction

It should be mentioned that in more realistic surgery operations, the trocar friction force may be applied to the slave robot. For this issue, friction identification and compensation mechanisms can be added to the proposed controller, which can be studied in future works. For this purpose, several methods were proposed in previous works on the friction compensation of robot manipulators considering mathematical fiction models (e.g., see [41-46]). Therefore, the identified friction force of trocar ($\mathbf{f}_{fric}$) should be obtained and subtracted from the measured slave force ($\mathbf{f}_{env}$), and then the resulted force ($\mathbf{f}_{env} - \mathbf{f}_{fric}$) should be employed as the pure slave-heart interaction force in the impedance models (8) and (9) instead of measured $\mathbf{f}_{env}$.

However, without any friction compensation (using the proposed strategy in this work), the slave robot will have a flexible behavior in response to the small trocar friction force using the designed slave impedance model (8). Another strategy for considering the trocar friction is employing a small force sensor to be placed after the trocar (at the tip of slave robot). In such configuration, the trocar friction can be considered in the term $\mathbf{F}_{\mathbf{x},s}(\dot{\mathbf{q}}_s)$ of the slave robot dynamics (4), and and the measured interaction force ($\mathbf{f}_{env}$) of the slave robot does not include the trocar friction.

6.5.3. Prevention of Large Slave-Heart Interaction Force

A large heart-robot interaction force may damage the heart tissue and should be avoided during the surgery operation. In the proposed strategy, the heart interaction force $\mathbf{f}_{env}$ is employed in the master impedance model (9). Therefore, this force is sensed by the surgeon via the master robot and can be controlled and decreased as much as needed by the surgeon force $\mathbf{f}_{sur}$, which affects the master and slave responses and consequently the heart-slave interaction.

On the other hand, due to the definition of the slave impedance model (8) in Sec. 3.1 and its appropriate adjustment in Sec. 3.2, the slave robot will track a deviation response $\tilde{\mathbf{x}}_{imp_s}$ (from the master robot trajectory) in response to the slave-heart interaction force $\mathbf{f}_{env}$. This performance prevents from generation of large interaction forces between the slave robot and the heart tissue. Because by increasing the force $\mathbf{f}_{env}$, the slave robot deviates more toward this interaction force (toward separation from the heart tissue), which decreases $\mathbf{f}_{env}$. In other words, the slave impedance model (8) as a mass-damper-spring system provides a flexibility for the slave robot in response to the heart interaction force. However, low and high values for the stiffness parameter k_s (and consequently other parameters) of this impedance model (8) are not appropriate as discussed in Sec. 3.2.

7. Conclusion

A force-based strategy for the teleoperation-assisted surgery of the beating heart was presented and tested via the proposed impedance control of the master and slave robots. In this strategy, without using any prediction and/or observation, compensation for the physiological heart motions is ensured. The oscillatory component of forces of the beating-heart is filtered out from the force feedback to surgeon's hand. Therefore, using this method, the human operator's sense (behaved as a surgeon) is similar to that experienced in arrested-heart surgery. These performances are achieved by the proposed adjustments to the desired master and slave impedance models. Moreover, the trade-offs for choosing the master and slave impedance parameters were explained for the robotic surgery on the beating heart.

Based on the Lyapunov stability proof, the designed nonlinear bilateral controller provides the tracking convergence to the impedance models' responses, in the presence of different modeling uncertainties. The experimental results confirmed the satisfactory performance of the proposed bilateral control strategy and its stability during the interaction with the beating heart. It was shown that using the appropriate impedance adjustment for the master and slave robots, the surgery is performed easily with normal and high heart-beat rates. However, it is demonstrated that the previous DFR control strategy with exact position and force tracking objectives is hard to be used for the same beating-heart surgery task which requires the manual oscillatory motion compensation by the operator (surgeon). Thus, the proposed strategy (with an automatic high-frequency motion compensation) can be used to perform future tele-robotic surgeries by real surgeons on the biological moving organs. However, the first step before implementation of the proposed strategy in human surgeries can be conducting some in-vivo animal experiments.

References

[1] A. M. Okamura, "Methods for haptic feedback in teleoperated robot-assisted surgery," *Industrial Robot: An International Journal*, vol. 31, no. 6, pp. 499-508, 2004.

[2] M. Sharifi, S. Behzadipour, H. Salarieh, and M. Tavakoli, "Cooperative modalities in robotic tele-rehabilitation using nonlinear bilateral impedance control," *Control Engineering Practice*, vol. 67, no. Supplement C, pp. 52-63, 2017.

[3] M. Najafi, M. Sharifi, K. Adams, and M. Tavakoli, "Robotic assistance for children with cerebral palsy based on learning from tele-cooperative demonstration," *International Journal of Intelligent Robotics and Applications*, vol. 1, no. 1, pp. 43-54, 2017.

[4] C. R. Carignan and H. I. Krebs, "Telerehabilitation robotics: Bright lights, big future?," (in English), *Journal of Rehabilitation Research and Development*, vol. 43, no. 5, pp. 695-710, 2006.

[5] F. Najafi and N. Sepehri, "Design and Prototyping of a Force-Reflecting Hand-Controller for Ultrasound Imaging," *Journal of Mechanisms and Robotics*, vol. 3, no. 2, p. 021002 (11 pages), 2011.

[6] M. Sharifi, H. Salarieh, S. Behzadipour, and M. Tavakoli, "Tele-echography of moving organs using an Impedance-controlled telerobotic system," *Mechatronics*, vol. 45, pp. 60-70, 2017.

[7] D. T. Kettler, R. D. Plowes, P. M. Novotny, N. V. Vasilyev, P. J. del Nido, and R. D. Howe, "An active motion compensation instrument for beating heart mitral valve surgery," in *Intelligent Robots and Systems (IROS), IEEE/RSJ International Conference on*, 2007, pp. 1290-1295.

[8] G. L. Reed, D. E. Singer, E. H. Picard, and R. W. DeSanctis, "Stroke Following Coronary-Artery Bypass Surgery," *New England Journal of Medicine*, vol. 319, no. 19, pp. 1246-1250, 1988.

[9] M. F. Newman *et al.*, "Longitudinal Assessment of Neurocognitive Function after Coronary-Artery Bypass Surgery," *New England Journal of Medicine*, vol. 344, no. 6, pp. 395-402, 2001.

[10] J. E. Colgate, "Robust impedance shaping telemanipulation," *Robotics and Automation, IEEE Transactions on*, vol. 9, no. 4, pp. 374-384, 1993.

[11] M. Tavakoli, R. V. Patel, M. Moallem, and A. Aziminejad, *Haptics For Teleoperated Surgical Robotic Systems*. World Scientific Publishing Co., Inc., 2008.

[12] M. Sharifi, S. Behzadipour, and H. Salarieh, "Nonlinear Bilateral Adaptive Impedance Control With Applications in Telesurgery and Telerehabilitation," *Journal of Dynamic Systems, Measurement, and Control*, vol. 138, no. 11, p. 111010 (16 pages), 2016.

[13] Y. C. Liu and N. Chopra, "Control of semi-autonomous teleoperation system with time delays," *Automatica*, vol. 49, no. 6, pp. 1553-1565, 2013.

[14] F. Hashemzadeh, M. Sharifi, and M. Tavakoli, "Nonlinear trilateral teleoperation stability analysis subjected to time-varying delays," *Control Engineering Practice*, vol. 56, pp. 123-135, 2016.

[15] Y. Nakamura, K. Kishi, and H. Kawakami, "Heartbeat synchronization for robotic cardiac surgery," in *Robotics and Automation (ICRA). Proceedings. IEEE International Conference on*, 2001, vol. 2, pp. 2014-2019.

[16] R. Ginhoux, J. Gangloff, M. de Mathelin, L. Soler, M. M. A. Sanchez, and J. Marescaux, "Active filtering of physiological motion in robotized surgery using predictive control," *Robotics, IEEE Transactions on*, vol. 21, no. 1, pp. 67-79, 2005.

[17] W. Bachta, P. Renaud, E. Laroche, A. Forgione, and J. Gangloff, "Active Stabilization for Robotized Beating Heart Surgery," *Robotics, IEEE Transactions on*, vol. 27, no. 4, pp. 757-768, 2011.

[18] O. Bebek and M. C. Cavusoglu, "Intelligent Control Algorithms for Robotic-Assisted Beating Heart Surgery," *Robotics, IEEE Transactions on*, vol. 23, no. 3, pp. 468-480, 2007.

[19] O. Bebek and M. C. Cavusoglu, "Whisker-Like Position Sensor for Measuring Physiological Motion," *IEEE/ASME Transactions on Mechatronics*, vol. 13, no. 5, pp. 538-547, 2008.

[20] A. Ataollahi, I. Berra, N. V. Vasilyev, Z. Machaidze, and P. E. Dupont, "Cardioscopic Tool-Delivery Instrument for Beating-Heart Surgery," *IEEE/ASME Transactions on Mechatronics*, vol. 21, no. 1, pp. 584-590, 2016.

[21] M. Bowthorpe, M. Tavakoli, H. Becher, and R. Howe, "Smith Predictor-Based Robot Control for Ultrasound-Guided Teleoperated Beating-Heart Surgery," *Biomedical and Health Informatics, IEEE Journal of*, vol. 18, no. 1, pp. 157-166, 2014.

[22] M. Bowthorpe and M. Tavakoli, "Physiological Organ Motion Prediction and Compensation Based on Multi-rate, Delayed, and Unregistered Measurements in Robot-assisted Surgery and Therapy," *Mechatronics, IEEE/ASME Transactions on*, vol. 21, no. 2, pp. 900-911, 2016.

[23] M. Kitagawa, A. M. Okamura, B. T. Bethea, V. L. Gott, and W. A. Baumgartner, "Analysis of Suture Manipulation Forces for Teleoperation with Force Feedback," in *Medical Image Computing and Computer-Assisted Intervention (MICCAI), International Conference on*, 2002, pp. 155-162.

[24] C. R. Wagner, N. Stylopoulos, P. G. Jackson, and R. D. Howe, "The Benefit of Force Feedback in Surgery: Examination of Blunt Dissection," *Presence: Teleoperators and Virtual Environments*, vol. 16, no. 3, pp. 252-262, 2007.

[25] Z. Zarrouk, A. Chemori, and P. Poignet, "Force feedback control for compensation of physiological motions in beating heart surgery with real-time experiments," in *Systems and Control (ICSC), 3rd International Conference on*, 2013, pp. 956-961.

[26] B. Cagneau, N. Zemiti, D. Bellot, and G. Morel, "Physiological Motion Compensation in Robotized Surgery using Force Feedback Control," in *Robotics and Automation (ICRA), IEEE International Conference on*, 2007, pp. 1881-1886.

[27] R. Cortesao and P. Poignet, "Motion compensation for robotic-assisted surgery with force feedback," in *Robotics and Automation (ICRA), IEEE International Conference on*, 2009, pp. 3464-3469.

[28] M. Dominici, P. Poignet, and E. Dombre, "Compensation of physiological motion using linear predictive force control," in *Intelligent Robots and Systems (IROS), IEEE/RSJ International Conference on*, 2008, pp. 1173-1178.

[29] M. Dominici, R. Cortesao, and C. Sousa, "Heart motion compensation for robotic-assisted surgery predictive approach vs. active observer," in *Robotics and Automation (ICRA), IEEE International Conference on*, 2011, pp. 6252-6257.

[30] M. Dominici and R. Cortesão, "Cascade force control for autonomous beating heart motion compensation," *Control Engineering Practice*, vol. 37, pp. 80-88, 2015.

[31] S. B. Kesner and R. D. Howe, "Robotic catheter cardiac ablation combining ultrasound guidance and force control," *The International Journal of Robotics Research*, vol. 33, no. 4, pp. 631-644, 2014.

[32] S. G. Yuen, D. P. Perrin, N. V. Vasilyev, P. J. del Nido, and R. D. Howe, "Force tracking with feed-forward motion estimation for beating heart surgery," *Robotics, IEEE Transactions on*, vol. 26, no. 5, pp. 888-896, 2010.

[33] S. Hasanzadeh and F. Janabi-Sharifi, "Model-Based Force Estimation for Intracardiac Catheters," *IEEE/ASME Transactions on Mechatronics*, vol. 21, no. 1, pp. 154-162, 2016.

[34] J. J. E. Slotine and W. Li, *Applied nonlinear control*. NJ, Englewood Cliffs: Prantice-Hall, 1991.

[35] X. Liu, R. Tao, and M. Tavakoli, "Adaptive control of uncertain nonlinear teleoperation systems," *Mechatronics*, vol. 24, no. 1, pp. 66-78, 2014.

[36] M. Sharifi, S. Behzadipour, and G. R. Vossoughi, "Model reference adaptive impedance control in Cartesian coordinates for physical human–robot interaction," *Advanced Robotics*, vol. 28, pp. 1277-1290, 2014.

[37] S. G. Yuen, N. V. Vasilyev, P. J. del Nido, and R. D. Howe, "Robotic tissue tracking for beating heart mitral valve surgery," *Medical Image Analysis*, vol. 17, no. 8, pp. 1236-1242, 2013.

[38] M. C. Çavuşoğlu, D. Feygin, and F. Tendick, "A Critical Study of the Mechanical and Electrical Properties of the PHANToM Haptic Interface and Improvements for High-Performance Control," *Presence: Teleoperators & Virtual Environments*, Article vol. 11, no. 6, pp. 555-568, 2002.

[39] M. D. Dyck, "Measuring the Dynamic Impedance of the Human Arm," M.Sc. Thesis, Department of Electrical and Computer Engineering, University of Alberta, 2013.

[40] M. Dyck and M. Tavakoli, "Measuring the dynamic impedance of the human arm without a force sensor," in *Rehabilitation Robotics (ICORR), IEEE International Conference on*, 2013, pp. 1-8.

[41] H. Olsson, K. J. Åström, C. Canudas de Wit, M. Gäfvert, and P. Lischinsky, "Friction Models and Friction Compensation," *European Journal of Control*, vol. 4, no. 3, pp. 176-195, 1998.

[42] B. Bona and M. Indri, "Friction Compensation in Robotics: an Overview," in *Proceedings of the 44th IEEE Conference on Decision and Control*, 2005, pp. 4360-4367.

[43] J. J. van den Dobbelsteen, A. Schooleman, and J. Dankelman, "Friction dynamics of trocars," *Surgical Endoscopy*, vol. 21, no. 8, pp. 1338-1343, 2007.

[44] L. L. Tien, A. Albu-Schaffer, A. D. Luca, and G. Hirzinger, "Friction observer and compensation for control of robots with joint torque measurement," in *IEEE/RSJ International Conference on Intelligent Robots and Systems*, 2008, pp. 3789-3795.

[45] M. Mahvash and A. Okamura, "Friction Compensation for Enhancing Transparency of a Teleoperator With Compliant Transmission," *IEEE Transactions on Robotics*, vol. 23, pp. 1240-1246, 2007.

[46] A. Alazmani, R. Roshan, D. G. Jayne, A. Neville, and P. Culmer, "Friction characteristics of trocars in laparoscopic surgery," *Proceedings of the Institution of Mechanical Engineers, Part H: Journal of Engineering in Medicine*, vol. 229, no. 4, pp. 271-279, 2015.